An improved computing method for the image edge detection

Gang Wang (王 刚)[1,2], Liang Xiao (肖 亮)[3], and Anzhi He (贺安之)[1]

[1]*School of Science, Nanjing University of Science & Technology, Nanjing 210094*

[2]*School of Physics & Electronics Engineering, Ludong University, Yantai 264025*

[3]*School of Computer Science & Technology, Nanjing University of Science & Technology, Nanjing 210094*

Received September 19, 2006

The framework of detecting the image edge based on the sub-pixel multi-fractal measure (SPMM) is presented. The measure is defined, which gives the sub-pixel local distribution of the image gradient. The more precise singularity exponent of every pixel can be obtained by performing the SPMM analysis on the image. Using the singularity exponents and the multi-fractal spectrum of the image, the image can be segmented into a series of sets with different singularity exponents, thus the image edge can be detected automatically and easily. The simulation results show that the SPMM has higher quality factor in the image edge detection.

OCIS codes: 100.2650, 100.5010, 100.2000, 120.2650.

The aim of image edge detection is the procedure of dividing the image into some regions with the particular attribute and extracting the interesting object. The traditional edge extraction operators are mainly based on the first and second derivative of the image gray level value[1]. However, the derivative of the gray level value is sensitive to the background noise. Moreover, when the images have lots of texture parts, they will be difficult to segment and to analyze with the traditional tools. In this paper, we adopt a multi-fractal approach, derived from thermodynamical concepts, which combines aspects from the physical and statistic attributes of the images to deal with the edge detection problem. Namely, due to the fact that a great variety of real world scenes are a flow in fully developed turbulence or chaotic nature images, we expect any intensive physical quantity to define a multi-fractal structure[2]. Then the images can be hierarchically decomposed into different parts from sharp edges to softer textures. From 90's up to the present, many researches on the multi-fractal methodology have been reported[3,4]. Through defining the measure μ as the gray level gradient integrating within every pixel neighborhood, Turiel *et al.* proposed the image multi-fractal decomposition method based on wavelet projection and the image reconstruction algorithm from the most singular manifold (MSM)[5,6]. In this paper, the new method is presented to extract the image edge by sub-pixel multi-fractal measure (SPMM). Compared with the traditional image detection algorithms, the proposed algorithm can obtain more precise results.

According to Ref. [7], any image is denoted as $I(\mathbf{x})$, where $\mathbf{x}$ is the vector coordinates of the referred pixel. For any subset Ω of the image, a positive measure $\mu(\Omega)$ is defined by

$$\mu(\Omega) = \int_{\Omega} \mathrm{d}\mathbf{y}\, |\nabla I|(\mathbf{y}), \tag{1}$$

where $|\nabla I(\mathbf{x})|$ denotes the modulus of the gray-level gradient $\nabla I(\mathbf{x})$. This measure gives an idea of the local variability of the gray level values around the point $\mathbf{x}$. According to the multi-fractal theory, we will be interested in the relationship between the measure and different scales. Given a collection of balls $B_r(\mathbf{x})$ of radii r centered at point $\mathbf{x}$, for r is small enough, if[5]

$$\mu(B_r(\mathbf{x})) \sim \alpha(\mathbf{x}) r^{d+h(\mathbf{x})}, \tag{2}$$

the measure is multi-fractal. Here the coefficient $\alpha(\mathbf{x})$ is scale independent and d is space dimension (the image dimension is 2). The local singularity exponent $h(\mathbf{x})$ characterizes the texture activity of the particular point $\mathbf{x}$. The exponents can be obtained by means of a log-log regression applied to Eq. (2) at every point. However, direct logarithmic regression performed on Eq. (2) yields rather coarse results when it is applied on discrete images, mainly due to the difficulties of interpolating the formula for scale r representing non-integer amounts of pixels. In such cases, it is convenient to study the projections of the measure $\mu(B_r(\mathbf{x}))$ over an appropriate wavelet $\psi(\frac{\mathbf{x}}{r})$ around the point $\mathbf{x}$[7]. If $\mu(B_r(\mathbf{x}))$ verifies Eq. (2) and the wavelets are the characteristic functions, tight support functions and prompt dropping functions[3], then the projection value has the exponential law with the scale r

$$T_{\psi}\mu(\mathbf{x_1}, r) \sim \beta(\mathbf{x_1}) r^{h(\mathbf{x_1})}, \tag{3}$$

where $\beta(\mathbf{x_1})$ is scale independent. Logarithmic regression performed on Eq. (3) yields the singularity exponent $(h(\mathbf{x_1}))$ of the particular point $\mathbf{x_1}$ representing from the most to the less informative structures of the image.

In order to acquire the precise value of the $h(\mathbf{x})$ of every point $\mathbf{x}$, a new algorithm is proposed to acquire the measure $\mu(B_r(\mathbf{x}))$ based on the gray level gradient $\nabla I(\mathbf{x})$ on the position of sub-pixel. First we apply the gradient operator on the contrast image: $\nabla \mathbf{I} = [G_x\ G_y]^{\mathrm{T}} = \left[\frac{\partial I}{\partial x}\ \frac{\partial I}{\partial y}\right]^{\mathrm{T}}$. Figure 1 shows the $B_r(\mathbf{x})$ with radii r circular neighborhood (gray region) and the pixels with rectangular domain. In general, the circular area does not only

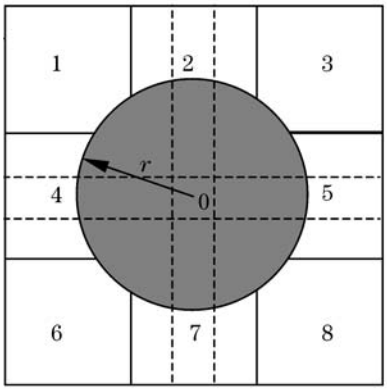

Fig. 1. Schematic plan of the radii r circular neighborhood.

contain integer-number pixels. As Fig. 1 shows that the circular area contains the other eight pixels besides pixel (No. 0). If we consider the gradient value of one pixel defined on the whole rectangular domain, the pixels on radii r circular neighborhood have different contributes for the measure $\mu(B_r(\mathbf{x}))$. So we need to divide the original pixel into the sub-pixels and calculate the gradient value at the position of the sub-pixels. For example, the pixel (No. 0) is divided into 9 sub-pixels by 3×3 lattice (see the dotted line in Fig. 1). In this way we can integrate the gradient value of every fraction contained in the $B_r(\mathbf{x})$. Owing to the convolution effect of charge coupled device (CCD) and optics diffraction processing, the sharp change in gray level value in object space will be transformed to gradual change in image space, i.e.

$$I(i,j) = \int_{j-0.5}^{j+0.5} \int_{i-0.5}^{i+0.5} g(x,y)\mathrm{d}x\mathrm{d}y, \tag{4}$$

where $I(i,j)$ denotes the gray value of the size of 1×1 unit pixel, $g(x,y)$ denotes the light distribution function. According to central-limit theorem, the gray level distribution law in the image can be assumed to be Gaussian distribution. So the wavelet projections $T_\psi\mu(\mathbf{x_1}, r)$ can be calculated by

$$T_\psi\mu(\mathbf{x_1}, r) = \int_{B_r(\mathbf{x})} [g'(\mathbf{y})\mathrm{d}\mu(\mathbf{y})] \frac{1}{r^d} \psi(\frac{\mathbf{x_1} - \mathbf{y}}{r}), \tag{5}$$

where $g'(\mathbf{y})$ denotes the gradient distribution coefficient at the point $\mathbf{y}$, and $\int_0^1 g'(r)\mathrm{d}r = 1$. The distribution coefficient $g'(\mathbf{y})$ at the position of the sub-pixels can be obtained by least square procedure applied on the known gradient value at integer position. Substituting Eq. (5) into Eq. (3), we can acquire the more precise $T_\psi\mu(\mathbf{x_1}, r)$ at the point $\mathbf{x_1}$. Given a wavelet, we compute for each image five wavelet projections at each point $\mathbf{x_1}$ for circular neighborhoods $B_{r_i}(\mathbf{x})\,|r_i = r_1, \cdots, r_5$. Then we perform a log-log linear regression according to Eq. (3). The slope equals the singularity exponent $h(\mathbf{x_1})$. Furthermore, the most singular exponent h_∞ is calculated as the average of the 1% and 5% quantile of the distribution of singular exponent. And the pixels belonging to $F_{h\infty} = F_{\mathrm{MSM}} = \{\mathbf{x}\,|h_\infty - \Delta h \le h(\mathbf{x}) \le h_\infty + \Delta h\}$ are collected into a set named by most singular manifold (MSM or 1th MSM). The choice dispersion value Δh is conventionally ± 0.15. Finally the MSM can be regarded as the contour of the image.

We apply the methodology above to decompose the image of Boston city (see Fig. 2, 256×256 pixels) into mutifractal components. Here the selected wavelet is the first radial derivative of Lorentzian wavelet $\psi(r) = \frac{-2r}{(1+r^2)^2}$ and the radii of the circular neighborhood take 1, $\sqrt{2}$, 2, $2\sqrt{2}$, 3 pixel size respectively. The original unit pixel is divided by 1×1, 3×3 lattice and the gradient distribution parameter is acquired by least square approximation. In order to compare the performance of SPMM (sub-pixel size of $1/(1 \times 1)$ and size of $1/(3 \times 3)$) with other classical edge detectors such as Prewitt operator and LoG (Laplacian-Gauss) operator, we make the results visible distinctly by transforming the processing results into binary images. The results are shown in Fig. 3. Figure 3(a) shows the result by utilizing the Prewitt operator (the default gray level gradient threshold is 0.04). Figure 3(b) shows the result of the LoG operator (the default gray level threshold is 0.0069, $\sigma = 2$). Figures 3(c) and (d) show the results of our SPMM method with sub-pixel size of $1/(1 \times 1)$ and $1/(3 \times 3)$, respectively. The singularity exponents are -0.53 and -0.445. From the above

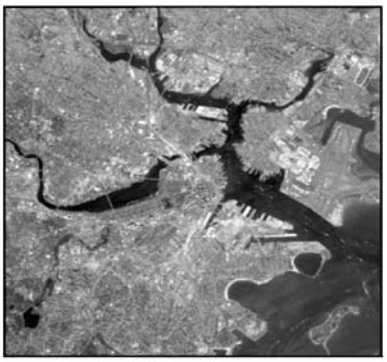

Fig. 2. Image of Boston city (256×256 pixels).

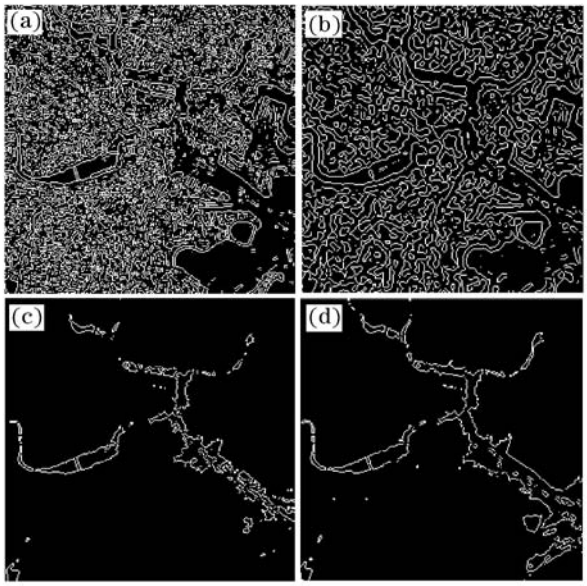

Fig. 3. Processing results of the image of Boston city using (a) sobel oprator, (b) LoG oprator, (c) SPMM method with sub-pixel size of $1/(1 \times 1)$, and (d) $1/(3 \times 3)$.

results, we can make conclusion that the edge extraction results based on multi-fractal measure are better than the classical edge detector. Moreover, owing to applying the SPMM method, the extracted edges preserve the details of the original image and the result agrees more with human visual observation. At the same time, the quality factors (Q factor) of the edge detectors mentioned above have been evaluated. According to the three error occurrence numbers (the edge pixels drop-out, locating the edge pixels failure, mistaking the noise pixels for the edge pixels) generated from the edge detection procedure, we define the Q factor as

$$Q = \frac{1}{N_{\mathrm{e}}} \sum_{i=1}^{N_{\mathrm{p}}} \frac{1}{1 + k d_i^2}, \tag{6}$$

where $N_{\mathrm{e}} = \max\{N_{\mathrm{I}}, N_{\mathrm{p}}\}$, N_{I}, N_{p} represent the pixel number of the ideal edge and the practical edge respectively, k is the proportional constant and d_i is the vertical distance between the practical edge point and the ideal edge point. The Gaussian noise (mean value = 0) is added into the test image (64×64 pixels, containing the vertical mark located in the middle of the image). The

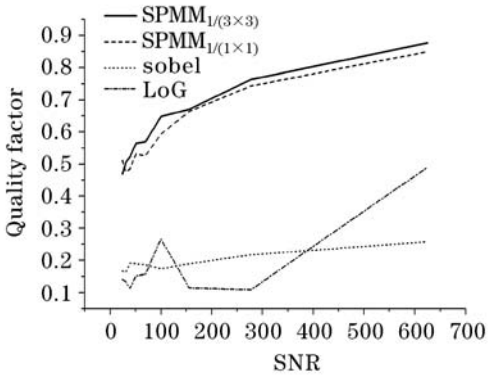

Fig. 4. Quality factor of the edge detectors and SNR.

Q factors of the detectors mentioned above are shown as Fig. 4. We define the signal-noise-ratio (SNR) as $(h/\sigma)^2$, here h indicates the edge contrast value and σ is the standard variance. From the figure, it is easy to see that the Q factor of SPMM edge detector is better than the others. This way indicates that the edge detector of SPMM has the good performance of the edge location.

The methodology of calculating the singularity exponents based on SPMM provides an efficient way for detecting the edge of images in rich of texture. The singularity exponents calculated by the multi-fractal formalism are very precise and reliable. The MSM points in the image detected by this way contain the most significant features of human visual system.

This work was supported by the Natural Science Foundation of China (No. 60672074), the Natural Science Foundation of Jiangsu Province (No. BK2006569), the Post Doctor Research Foundation of China (No. 20060390285 and 20060601005B), and the Youth Foundation of Nanjing University of Science and Technology (No. NJUST200401). G. Wang's e-mail address is happy_wg@163.com.

References

1. Z.-M. Ma and C.-K. Tao, Chin. J. Lasers (in Chinese) **27,** 237 (2000).
2. Z. Hou and Y. Qin, Acta Opt. Sin. (in Chinese) **22,** 210 (2002).
3. Z.-L. Xia, Z.-X. Fan, and J.-D. Shao, Chin. J. Lasers (in Chinese) **33,** 111 (2006).
4. N. Decoster, S. G. Roux, and A. Arnéodo, Eur. Phys. J. B. **15,** 739 (2000).
5. A. Turiel, G. Mato, and N. Parga, Phys. Rev. Lett. **80,** 1098 (1998).
6. A. Turiel and A. del Pozo, IEEE Trans. Image Processing **11,** 345 (2002).
7. A. Turiel and N. Parga, Neural Computation **12,** 763 (2000).